

Simultaneous estimation of global present-day water transport and glacial isostatic adjustment

Xiaoping Wu^{1*}, Michael B. Heflin¹, Hugo Schotman^{2,3}, Bert L. A. Vermeersen², Danan Dong¹, Richard S. Gross¹, Erik R. Ivins¹, Angelyn W. Moore¹ and Susan E. Owen¹

Global water transport between oceans and continents during the transition from glacial to interglacial times has been enormous. The viscoelastic solid Earth has been responding to this unloading of large ice masses with a rise of the land masses, in a process termed glacial isostatic adjustment. In addition, significant changes in the land/ocean water distribution occur at present. As both present-day changes in the ice/water thickness and glacial isostatic adjustment affect space geodetic measurements, it is difficult to untangle the relative contributions of these two processes. Here we combine gravity measurements and geodetic data of surface movement with a data-assimilating model of ocean bottom pressure to simultaneously estimate present-day water transport and glacial isostatic adjustment. We determine their separate contributions to movements in the geocentre, which occur in response to changes in the Earth's mass distribution, with uncertainties below 0.1 mm yr^{-1} . According to our estimates, mass losses between 2002 and 2008 in Greenland, Alaska/Yukon and West Antarctica are 104 ± 23 , 101 ± 23 and $64 \pm 32 \text{ Gt yr}^{-1}$, respectively. Our estimates of glacial isostatic adjustment indicate a large geocentre velocity of $-0.72 \pm 0.06 \text{ mm yr}^{-1}$ in the polar direction. We conclude that a significant revision of the present estimates of glacial isostatic adjustments and land-ocean water exchange is required.

Strong evidence for present-day surface mass trend (PDMT) has emerged from satellite tracking and other data^{1–13}, especially from the Gravity Recovery and Climate Experiment (GRACE) mission^{3–8}. Still, separating PDMT and glacial isostatic adjustment^{14–16} (GIA) signatures in most high-precision geodetic data is a major challenge¹⁷. Unknown but possibly significant uncertainties remain about ice history^{14,15} and the rheological profile of the Earth^{14,15,18–20} in the GIA models. Estimating GIA in Greenland and Antarctica is particularly difficult owing to very sparse near-field relative sea level records. At present, PDMT is estimated by correcting GRACE and other data using recent GIA models^{4–8}, and GIA over certain regions is studied by correcting the data using hydrological models²¹. Potentially large errors in the models will be aliased into the resulting PDMT or GIA estimates. Both PDMT (ref. 22) and GIA (refs 23,24) also drive geocentre velocities of the centre-of-mass of the total Earth system with respect to the centre-of-figure of the solid Earth surface. Such velocities and their underlying degree-1 spherical harmonic surface mass variations have not been reliably determined from observations²⁵, but are integral and important parts of the global change spectra. These motivated us to estimate PDMT and GIA simultaneously in a global inverse study with a realistic and fairly rigorous uncertainty assessment.

From April 2002 to December 2008, linear trends are derived from GRACE gravity data with empirically calibrated full covariance matrices²⁶, and from the Jet Propulsion Laboratory's data-assimilating ocean bottom pressure (OBP) model²⁷. These are combined with three-dimensional surface velocities at 664 globally distributed sites. Although the durations of the surface geodetic time series are diverse, most of the data are collected by the global positioning system (GPS) technique during the 2000s and processed

up to August 2007. Spherical harmonic coefficients of both PDMT and GIA signatures as well as other relevant parameters are then estimated from the data combination (see the Methods section).

Separate long-wavelength signatures

Table 1 lists geocentre velocities (V_G) and a few low-degree dimensionless geopotential coefficients of considerable historic interest owing to PDMT (including the atmospheric mass) and GIA. The y component owing to PDMT is clearly significant. Overall, the geocentre velocity owing to PDMT is small, which is not known *a priori*. Still, the seemingly very small z component contributes a 13 Gt yr^{-1} mass gain for Antarctica when supplemented to the GRACE data. The Earth's dynamic oblateness rate \dot{J}_2 owing to PDMT shows a larger positive value than the absolute value of the negative \dot{J}_2 owing to GIA, resulting in a net increase in the Earth's oblateness during 2002–2008. A similar behaviour was observed in the late 1990s (ref. 1). The GIA estimates show a very significant $-0.72 \pm 0.06 \text{ mm yr}^{-1}$ contribution to the geocentre velocity along the z axis compared with -0.48 mm yr^{-1} in the *a priori* GIA

Table 1 | Estimated long-wavelength geodetic signatures and uncertainties.

Component	PDMT estimate	GIA estimate
V_{GX} (mm yr^{-1})	-0.08 ± 0.04	-0.10 ± 0.01
V_{GY} (mm yr^{-1})	0.29 ± 0.05	0.11 ± 0.02
V_{GZ} (mm yr^{-1})	-0.16 ± 0.07	-0.72 ± 0.06
\dot{J}_2 (yr^{-1})	$(5.2 \pm 0.5) \times 10^{-11}$	$(-3.4 \pm 0.4) \times 10^{-11}$
\dot{J}_3 (yr^{-1})	$(1.3 \pm 0.4) \times 10^{-11}$	$(0.6 \pm 0.3) \times 10^{-11}$

¹Jet Propulsion Laboratory, California Institute of Technology, Mail Stop 238-600, 4800 Oak Grove Drive, Pasadena, California 91109, USA, ²DEOS, Faculty of Aerospace Engineering, Delft University of Technology, Kluyverweg 1, Delft, 2629 HS, Netherlands, ³SRON Netherlands Institute for Space Research, Sorbonnelaan 2, Utrecht, 3584 CA, Netherlands. *e-mail: Xiaoping.Wu@jpl.nasa.gov.

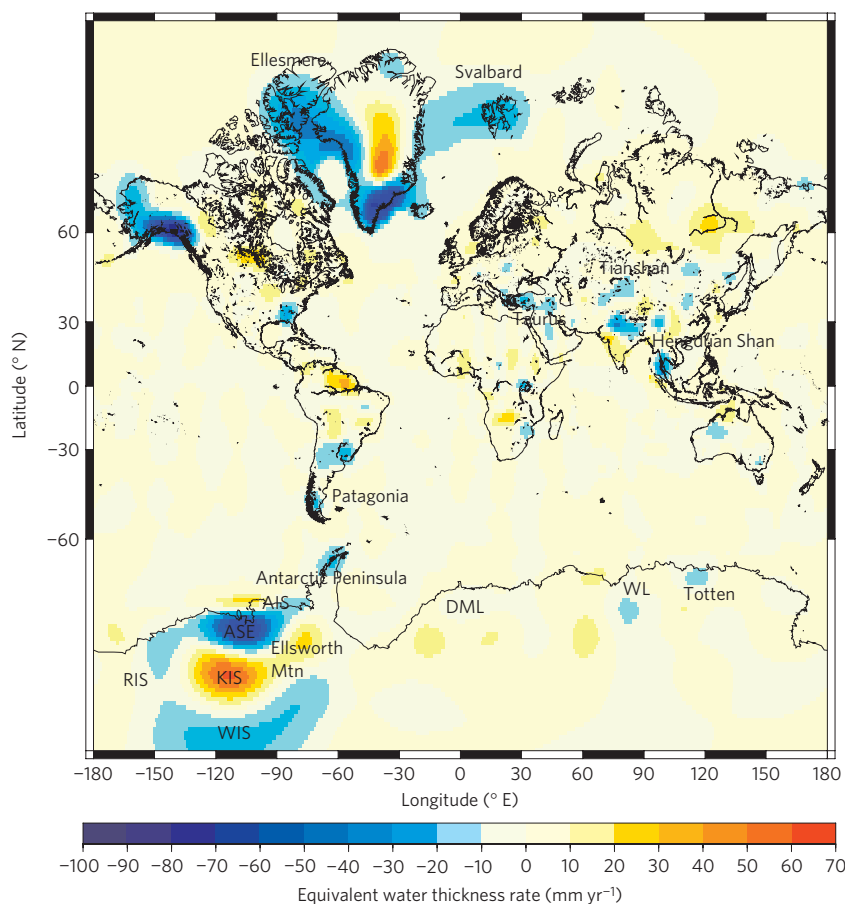


Figure 1 | Average global PDMT estimates including the atmospheric mass in thickness of water equivalent. An optimal averaging function at each grid point is used with a similar resolution to that of the 300-km Gaussian spatial filter but a smaller uncertainty. AIS (Abbott Ice Shelf), ASE (Amundsen Sea embayment), DML (Dronning Maud Land), KIS (Kamb Ice Stream), RIS (Ross Ice Shelf), Totten (Glacier), WIS (Whillans Ice Stream), WL (Wilkes Land).

model^{14,15}. These newly determined geocentre velocity components owing to GIA can be used in future dynamic studies to further improve our understanding of the ice history and Earth rheology on a global scale. Our GIA \dot{J}_2 estimate is fairly close to that of the *a priori* GIA model ($-3.9 \times 10^{-11} \text{ yr}^{-1}$) and not far from the long-term (33 years) satellite laser ranging (SLR) observations² of $-2.75 \times 10^{-11} \text{ yr}^{-1}$. As the observed long-term \dot{J}_2 is the sum of GIA and the long-term PDMT contributions, our result indicates that the latter is limited to around $0.65 \times 10^{-11} \text{ yr}^{-1}$, subject to an additional uncertainty associated with the removal of the 18.6 year solid Earth tide²⁸.

Global spatial pattern of present-day surface mass trend

The inverted PDMT coefficients including the atmospheric mass are sensed by the GRACE and GPS data, and do not directly depend on any atmospheric analysis. These coefficients and their covariance matrix are then used to compute optimal spatial average values around global $1^\circ \times 1^\circ$ grid points²⁶ (see the Methods section). The averaging results and their uncertainties are shown in Fig. 1 and Supplementary Fig. 1, respectively. Intensive ice melting can be seen in the southern area of Alaska/Yukon, including Bering and Malaspina glaciers, Yakutat Icefield and Glacial Bay, in agreement with recent studies based on local glaciological/GPS uplift¹⁸ and GRACE data^{6,7}. On the other hand, we also find significant mass loss along the west coast of Alaska with no appreciable changes in the interior. The mass loss in Greenland is concentrated along the coastal areas, and is particularly heavy in the west, and in the southeast with the large Kangerdlugssuaq and Helheim glaciers. Significant losses can also be seen over

Svalbard and Ellesmere Island where mass losses through calving and surface ablation have been reported before by surface, radar and imagery observations⁹. In contrast, the interior of Greenland shows significant positive mass balance. The image of inland thickening, owing to increased precipitation, and coastal thinning, owing to enhanced surface melting and ice dynamics, is in very good agreement with recent altimetry studies^{10,11} and in line with the predicted ice-sheet response to climate warming. In particular, the average $24\text{--}38 \text{ mm yr}^{-1}$ thickening above 2000 m elevation during 1993–2004 from laser altimeters¹⁰ is very close to our interior results. Areas of both intensive gain and loss are found in West Antarctica, including the northern tip of the Antarctic Peninsula, whereas East Antarctica seems fairly stable. Although independent and with a lower spatial resolution, our Antarctic mass trends show similar significant features identified as ice- or snow-mass changes by a recent European remote sensing (ERS) satellite altimeter study¹² and by Ice, Cloud and land Elevation Satellite (ICESat) laser altimeter observations^{11,13}. These include the significant drawdown of the glaciers in the Amundsen Sea sector; the thickening further inland of the sector confirming the shutdown of Kamb Ice Stream, in the coastal area east of Amundsen Sea embayment feeding the Abbott Ice Shelf; and in the Ellsworth Mountains region south of the Antarctic Peninsula. In addition, our results seem to support the full ICESat picture of Kamb Ice Stream thickening, and thinning in the tributary region of Whillans Ice Stream as well as along the east coast of the Ross Ice Shelf^{11,13}. In other areas of Antarctica where thickening and thinning are indicated by the ERS and ICESat data, some qualitative agreements can also be found in our results (for example, some thickening in the western portion of Dronning

Table 2 | Regional mean present-day mass trend.

Region	Mass gain all data (GIA estimated) Gt yr ⁻¹	Mass gain GRACE only (GIA corrected) Gt yr ⁻¹	Mass gain other GRACE estimates Gt yr ⁻¹
Greenland	-104 ± 23	-161 ± 35	-234 ± 33 (ref. 4)
Alaska/Yukon	-101 ± 23	-68 ± 28	-91 ± 5 (ref. 7)
West Antarctica	-64 ± 32	-99 ± 59	-130 ± 26 (ref. 5)
East Antarctica	-23 ± 29	16 ± 54	-45 ± 52 (ref. 5)
Remaining land	14 ± 76	-74 ± 148	E + W (ref. 4) = -132 ± 73
Oceans	236 ± 81	341 ± 137	
Non-steric (mass) mean sea level	Global ±66°	0.54 ± 0.3 mm yr ⁻¹ 0.70 ± 0.3 mm yr ⁻¹	0.82 ± 0.4 mm yr ⁻¹ 0.94 ± 0.4 mm yr ⁻¹
			0.8 ± 0.5 mm yr ⁻¹ (ref. 32)

The estimated regional mass gains include the atmospheric contributions. Atmospheric contributions were removed in the original referenced GRACE estimates, and are restored here for comparison except in the mean sea level³², using the same European Centre for Medium-Range Weather Forecasts operational analysis surface pressure data (Supplementary Table S1). 37.4 Gt yr⁻¹ corresponds to 0.1 mm yr⁻¹ equivalent mean sea level. The non-steric mean sea level estimates are calculated by removing the atmospheric contribution and are subject to its uncertainty of ~0.2 mm yr⁻¹. The mean sea level result within the ±66° latitude band is to be compared with Jason-1 data.

Maud Land and thinning in Totten Glacier). However, our results do not show significant thickening in the coastal area of Wilkes Land observed by the ERS altimetry data¹² (1993–2002), which is not supported by snow accumulation data¹² or the ICESat result¹¹. Our PDMT pattern in West Antarctica is similar to that of a recent study using almost the same amount of GRACE data⁵, except in the coastal area east of Amundsen Sea embayment feeding the Abbott Ice Shelf. The difference may be attributed to the improvement from the OBP data and the optimal filter.

The optimal averaging function is especially powerful in identifying geographically isolated mass variations and allows us to see mass losses of many mountain glaciers shown on the map including Tianshan, Hengduan Shan, Patagonia, Anti-Taurus and Taurus. Other remarkable features are several areas of mass increases on the continents, including those in the Amazon, Lena, Nelson and Zambezi basins, and mass losses owing to groundwater depletion in northern India and droughts in southeastern United States and South America. The aliased signature of the 2004 Sumatra earthquake (not removed from the data) can also be seen.

Geographic budget of present-day surface mass trend

A budget of PDMT over major geographic regions of the world (Table 2) is computed by using optimal regional averaging functions and the inverted PDMT coefficients (including the atmospheric mass) sensed by the data. During 2002–2008, the thinning ice sheets and mountain glaciers contributed significantly to sea level rise. For example, the total mass loss over the two ice sheets and Alaska/Yukon (west of 130° W) would correspond to a 0.78 mm yr⁻¹ non-steric sea level rise. However, the remaining land area shows a small net gain in mass despite losses over the mountain glaciers and ice caps. This is not surprising as evaporation, atmospheric circulation and precipitation processes can transport water mass (including from the oceans) over large distances around the globe (see also ref. 29). For comparison, a GRACE-only PDMT solution is also listed, with GIA corrected using the fixed *a priori* model including its covariance matrix and supplemental degree-1 information from a multiple data inversion. The large differences (mostly over the ice-covered areas) of our two PDMT solutions and the larger uncertainties of the GIA-corrected solution demonstrate the importance of GIA model improvement and enhanced resolution/accuracy resulting from the data combination. Whereas the Alaska mass loss agrees with a recent GRACE study having the data-constrained GIA effect corrected⁷, our PDMT estimates over Greenland and Antarctica are considerably different from some other GRACE estimates (ref. 30 and fourth column of Table 2, where the atmospheric contributions removed by the authors have been restored except in the case of non-steric mean sea

level). Differences in the treatment of GIA, atmospheric mass and GRACE data, especially over long-wavelength coefficients (such as degree-1 or 2) and differing time spans can play significant roles. For example, an earlier GRACE mass concentration study⁸ using three years of data and a GIA correction yielded a Greenland result similar to our estimate. However, two recent studies using essentially the same span of GRACE data as ours reported larger (about a factor of 2) mass losses for Greenland⁴ and Antarctica^{4,5}. With other subtle differences in data handling, their methods and results are in general agreement (within the range of uncertainties) with our GIA-corrected GRACE-only estimates. Therefore, we conclude that our smaller mass loss estimates for Greenland and Antarctica are due to GIA improvement and enhanced resolution and accuracy from the data combination. We also note that our results are generally in better agreement with altimetry (over different periods)^{10–13,30} than with other GRACE estimates.

To derive non-steric mean sea level rise, atmospheric mass contribution over the oceans is removed using the National Centers for Environmental Prediction reanalysis-2 surface pressure data (Supplementary Table S1) with an additional uncertainty of ~0.2 mm yr⁻¹ (70 Gt yr⁻¹) from the pressure data³¹ (Supplementary Information). When compared to the 2.4 ± 1.1 mm yr⁻¹ total mean sea level rise determined from Jason-1 altimetry (between ±66° latitudes) using a GIA correction and a steric contribution of 0.8 ± 0.8 mm yr⁻¹ (ref. 32), our 0.7 ± 0.3 mm yr⁻¹ (similar to that of ref. 32) non-steric mean sea level rise estimate (between ±66° latitudes) is well within the range of uncertainties, particularly considering the slightly different time spans. Our mean sea level rise estimate over the global oceans is smaller because during 2002–2008 the semi-enclosed Arctic Ocean has a significant mass loss according to our PDMT estimate (-91 ± 15 Gt yr⁻¹), which may be linked to the decadal oceanographic variability of freshwater release of the Arctic ‘capacitor’³³.

Estimated glacial isostatic adjustment

As shown in Fig. 2, the pattern of estimated GIA-induced geoid rate over Laurentia is slightly different from that of the *a priori* model (ICE-5G in the Northern Hemisphere). A large negative geoid trend in the middle of Greenland is seen where a pronounced positive PDMT is also found in our solution. The trend is significant with a maximum signal-to-noise ratio of 4 (Fig. 2a, Supplementary Fig. S2). The mean GIA geoid trend over Greenland calculated using a simple box-car averaging function is -0.56 ± 0.17 mm yr⁻¹, rather than 0.1 ± 0.35 mm yr⁻¹ as suggested by the *a priori* model. Our uncertainty estimates, which also peak in the middle of the Greenland and Antarctic ice sheets, are fairly rigorous. Simulated inverse recoveries reveal no algorithm artefact. Therefore, part

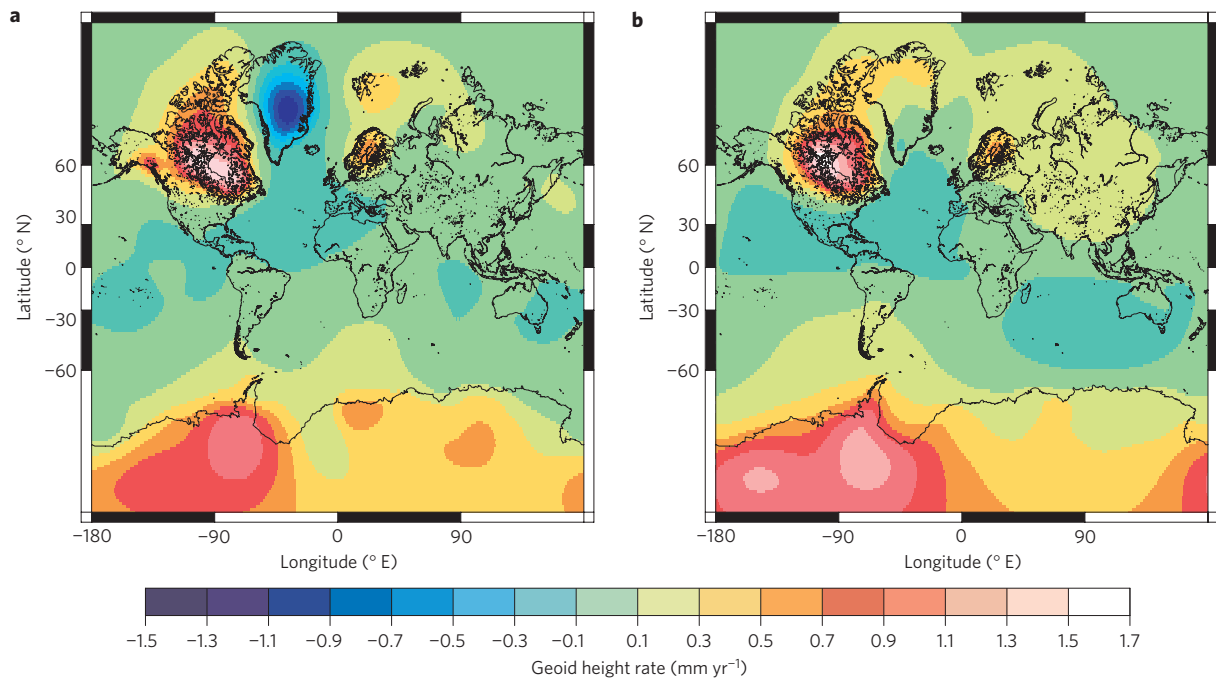


Figure 2 | Unfiltered GIA geoid height trends. a, Estimated in this study. **b**, Predicted by ICE-5G/IJ05/VM2 model.

of the negative GIA geoid trend in Greenland could be new evidence for additional net past ice accumulation ($\sim 100\text{--}300$ m of ice depending on rheological properties and onset time) in comparison with the *a priori* model. Past accumulation over certain parts of Greenland has been suggested before by other data and dynamic ice models^{14,34}. The GIA solution contains a strong rebound over Alaska. This is a feature not found in the *a priori* model, and provides support for regional inferences of significant ice melting since the Little Ice Age¹⁸. In Antarctica, our GIA solution agrees better on average with the *a priori* model, but a slightly weaker mean GIA signature is found in West Antarctica. Like the *a priori* GIA model, our estimated GIA-induced geoid trends can be removed from the GRACE data for users interested in determining PDMT. For GRACE sea level determination, removing the estimated negative GIA geoid trends corresponds to adding $0.66 \pm 0.1 \text{ mm yr}^{-1}$ (global oceans) and $0.82 \pm 0.1 \text{ mm yr}^{-1} (\pm 66^\circ)$ to the raw results, compared with 0.95 mm yr^{-1} (global) and $1.1 \text{ mm yr}^{-1} (\pm 66^\circ)$ suggested by the *a priori* model.

Implications and perspectives

The simultaneous kinematic global inversion presented here allows us to separate the global PDMT and GIA signatures in the geodetic data with unprecedented precision. These results are achieved by combining the multi-satellite high-precision geodetic data with the *a priori* information on GIA dynamics and the relatively well-constrained spatial extent of deglaciation from glacio-geological data. The GIA improvement and the enhanced resolution and accuracy from the data combination result in (about a factor of two) smaller mass loss estimates for Greenland and Antarctica during 2002–2008 than other recent GIA-corrected GRACE estimates. The non-steric mean sea level rise is estimated to be $0.54 \pm 0.3 \text{ mm yr}^{-1}$ (global) and $0.70 \pm 0.3 \text{ mm yr}^{-1} (\pm 66^\circ)$. The time span of the geodetic data, however, is still short. For example, the SLR-observed \dot{J}_2 during 2002–2008 greatly contradicts that of the longer-term (33 years) SLR tracking data. This indicates that the estimated PDMT in \dot{J}_2 or any other PDMT coefficients may be interannual or decadal in nature rather than a century-scale secular trend. Our GIA estimates reveal significant new features in areas where GIA models are known to be poor. The largest uncertainty values

are over the interiors of Greenland and Antarctica where spatially coherent data fusion is lacking. In the coming decade, as time series of global gravity, altimetry and GPS continue to improve, better constraints on ice-sheet mass balances and their contributions to sea level shall be achieved.

Methods

Global inversion. The theoretical framework (including the relevant measurement equations), data sets and uncertainty assessment are described in the Supplementary Information. We take a kinematic approach to the simultaneous estimation problem. GRACE gravitational geoid (referred to as geoid hereafter) trend and surface velocities both have PDMT and GIA components, whereas the OBP data have only a PDMT component. The horizontal velocities also have a plate motion component. The measurement equations of the data correspond largely to separate spherical harmonic expansions of the PDMT and GIA components. The coefficients of the PDMT components of all three data types are completely described by the PDMT coefficients. The GIA components, on the other hand, are described by separate coefficients of geoid trend, vertical and horizontal surface velocities. We solve for separate spherical harmonic coefficients of PDMT, and of vertical and horizontal GIA respectively, from degree $n = 1$ to 60, GIA geoid harmonic coefficients from $n = 2$ to 7 and rotation vectors of 15 major tectonic plates. The GIA geoid coefficients from $n = 8$ to 60, to a good precision, are approximately related to the corresponding vertical coefficients¹⁷, and are substituted by the latter in the measurement equations to reduce the size of the problem. The kinematic approach resolves PDMT without the complication of estimating load-time history^{14,15,18} and Earth's rheological profile^{18–20}, which cannot be completely resolved by modern geodetic data alone. The dynamics and our prior knowledge of the GIA process are incorporated in the inversion through the use of *a priori* information, which consists of *a priori* mean values and an *a priori* covariance matrix of all GIA parameters. We use the average of ICE-5G (ref. 14)/IJ05 (ref. 15) ice-history models and the VM2 (ref. 14) Earth rheology profile to compute the *a priori* mean values. The *a priori* covariance matrix is constructed dynamically assuming large but plausible uncertainties in ice history and Earth rheology (Supplementary Information). No effective *a priori* knowledge is used for other parameters in the inverse problem, which is solved by the method of least squares with reduced *a priori* information³⁵. The inverse method also yields a full covariance matrix for all of the estimated parameters.

Optimal averaging functions. Once the spherical harmonic coefficients of PDMT are estimated, an optimal averaging function around each grid point is constructed to minimize the uncertainty in the average value with a fixed level of spatial resolution using the estimated full covariance matrix of the PDMT coefficients. With the same spatial resolution as that of the 300-km Gaussian average, the optimal functions result in much smaller uncertainties²⁶. For a water storage budget of the major geographic areas of the world, optimal regional averaging functions

are constructed using the least-squares method incorporating *a priori* information to minimize the total error resulting from measurement noises and signal leakage. A zero *a priori* mean value is assumed in all cases. Global homogeneous Gaussian *a priori* covariance functions having a 400-km correlation length are used to construct averaging functions over land areas, with a 20 cm yr⁻¹ uncertainty for the ice sheets and Alaska/Yukon, and a 10 cm yr⁻¹ uncertainty for the rest of ice-free land, respectively. To construct an optimal averaging function over the oceans, a two-region Gaussian *a priori* covariance function with independent variation regimes (with 2 cm yr⁻¹ and 15 cm yr⁻¹ uncertainties for the oceans and land respectively) is used. Mass variations within the oceans or the land areas are assumed correlated spatially with a 400-km correlation length. However, across the ocean/land boundary, mass variations are independent from each other. Two additional constraints are applied *a priori* such that the average weights over the surface of the Earth and over the region of interest are both unity²⁶. The GIA-induced geoid change is derived as a simple sum of the spherical harmonic components up to degree and order 60, because the *a priori* GIA information acts as an efficient low-pass filter.

Received 12 January 2010; accepted 16 July 2010; published online 15 August 2010

References

- Cox, C. M. & Chao, B. F. Detection of a large-scale mass redistribution in the terrestrial system since 1998. *Science* **297**, 831–833 (2002).
- Cheng, M. & Tapley, B. D. Variations in the Earth's oblateness during the past 28 years. *J. Geophys. Res.* **109**, B09402 (2004).
- Tapley, B. D., Bettadpur, S., Ries, J. C., Thompson, P. F. & Watkins, M. M. GRACE measurements of mass variability in the Earth system. *Science* **305**, 503–505 (2004).
- Velicogna, I. Increasing rates of ice mass loss from the Greenland and Antarctic ice sheets revealed by GRACE. *Geophys. Res. Lett.* **36**, L19503 (2009).
- Chen, J. L., Wilson, C. R., Blankenship, D. & Tapley, B. D. Accelerated Antarctic ice loss from satellite gravity measurements. *Nature Geosci.* **2**, 859–862 (2009).
- Tamisiea, M. E., Leuliette, E. W., Davis, J. L. & Mitrovica, J. X. Constraining hydrological and cryospheric mass flux in southern Alaska using space-based gravity measurements. *Geophys. Res. Lett.* **32**, L20501 (2005).
- Luthcke, S. B. *et al.* Recent glacier mass changes in the Gulf of Alaska region from GRACE mascon solutions. *J. Glaciol.* **54**, 767–777 (2008).
- Luthcke, S. B. *et al.* Recent Greenland ice mass loss by drainage system from satellite gravity observations. *Science* **314**, 1286–1289 (2006).
- Dowdeswell, J. A., Benham, T. J., Strozzi, T. & Hagen, J. O. Iceberg calving flux and mass balance of the Austfonna ice cap on Nordaustlandet, Svalbard. *J. Geophys. Res.* **113**, F03022 (2008).
- Thomas, R., Frederick, E., Krabill, W., Manizade, S. & Martin, C. Progressive increase in ice loss from Greenland. *Geophys. Res. Lett.* **33**, L10503 (2006).
- Pritchard, H. D., Arthern, R. J., Vaughan, D. G. & Edwards, L. A. Extensive dynamic thinning on the margins of the Greenland and Antarctic ice sheets. *Nature* **461**, 971–975 (2009).
- Wingham, D. J., Shepherd, A., Muir, A. & Marshall, G. J. Mass balance of the Antarctic ice sheet. *Phil. Trans. R. Soc. A* **364**, 1627–1635 (2006).
- Smith, B. E., Bentley, C. R. & Raymond, C. F. Recent elevation changes on the ice streams and ridges of the Ross Embayment from ICESat crossovers. *Geophys. Res. Lett.* **32**, L21S09 (2005).
- Peltier, W. R. Global glacial isostasy and the surface of the ice-age Earth: The ICE-5G (VM2) model and GRACE. *Annu. Rev. Earth Planet. Sci.* **32**, 111–149 (2004).
- Ivins, E. R. & James, T. S. Antarctic glacial isostatic adjustment: A new assessment. *Antarct. Sci.* **17**, 537–549 (2005).
- Vermeersen, L. L. A. & Sabadini, R. A new class of stratified viscoelastic models by analytical techniques. *Geophys. J. Int.* **129**, 531–570 (1997).
- Wahr, J., Wingham, D. & Bentley, C. A method of combining ICESat and GRACE satellite data to constrain Antarctic mass balance. *J. Geophys. Res.* **105**, 16279–16294 (2000).
- Larsen, C. F., Motyka, R. J., Freymueller, J. T., Echelmeyer, K. A. & Ivins, E. R. Rapid viscoelastic uplift in southeast Alaska caused by post-Little Ice Age glacial retreat. *Earth Planet. Sci. Lett.* **237**, 548–560 (2005).
- Wieczerkowski, K., Mitrovica, J. X. & Wolf, D. A revised relaxation-time spectrum for Fennoscandia. *Geophys. J. Int.* **139**, 69–86 (1999).
- James, T. S., Gowan, E. J., Wada, I. & Wang, K. Viscosity of the asthenosphere from glacial isostatic adjustment and subduction dynamics at the northern Cascadia subduction zone, British Columbia, Canada. *J. Geophys. Res.* **114**, B04405 (2009).
- Tamisiea, M. E., Mitrovica, J. X. & Davis, J. L. GRACE gravity data constrain ancient ice geometries and continental dynamics over Laurentia. *Science* **316**, 881–883 (2007).
- Trupin, A. S., Meier, M. F. & Wahr, J. M. Effects of melting glaciers on the Earth's rotation and gravitational field: 1965–1984. *Geophys. J. Int.* **108**, 1–15 (1992).
- Greff-Lefertz, M. Secular variation of the geocenter. *J. Geophys. Res.* **105**, 25685–25692 (2000).
- Klemann, V. & Martinec, Z. Contribution of glacial-isostatic adjustment to the geocenter motion. *Tectonophysics* doi:10.1016/j.tecto.2009.08.031 (2009), in the press.
- Altamimi, Z., Collilieux, X., Legrand, J., Garayt, B. & Boucher, C. ITRF2005: A new release of the international terrestrial reference frame based on time series of station positions and Earth orientation parameters. *J. Geophys. Res.* **112**, B09401 (2007).
- Wu, X., Blom, R. G., Ivins, E. R., Oyafuso, F. A. & Zhong, M. Improved inverse and probabilistic methods for geophysical applications of GRACE gravity data. *Geophys. J. Int.* **177**, 865–877 (2009).
- Fukumori, I., Raghunath, R., Fu, L. & Chao, Y. Assimilation of TOPEX/POSEIDON data into a global ocean circulation model: How good are the results? *J. Geophys. Res.* **104**, 25647–25665 (1999).
- Benjamin, D., Wahr, J., Ray, R. D., Egbert, G. D. & Desai, S. D. Constraints on mantle anelasticity from geodetic observations, and implications for the J_2 anomaly. *Geophys. J. Int.* **165**, 3–16 (2006).
- Chao, B. F., Wu, Y. H. & Li, Y. S. Impact of artificial reservoir water impoundment on global sea level. *Science* **320**, 212–214 (2008).
- Shepherd, A. & Wingham, D. Recent sea-level contributions of the Antarctic and Greenland ice sheets. *Science* **315**, 1529–1532 (2007).
- Trenberth, K. & Smith, L. The mass of the atmosphere: A constraint on global analyses. *J. Clim.* **18**, 864–875 (2005).
- Leuliette, E. W. & Miller, L. Closing the sea level rise budget with altimetry, Argo, and GRACE. *Geophys. Res. Lett.* **36**, L04608 (2009).
- Steele, M. & Ermold, W. Steric sea level change in the Northern Seas. *J. Clim.* **20**, 403–417 (2007).
- Sparrenbom, C. J., Bennike, O., Bjorck, S. & Lambeck, K. Relative sea-level changes since 15,000 cal. yr BP in the Nanortalik area, southern Greenland. *J. Quat. Sci.* **21**, 29–48 (2006).
- Wu, X., Heflin, M. B., Ivins, E. R. & Fukumori, I. Seasonal and interannual global surface mass variations from multisatellite geodetic data. *J. Geophys. Res.* **111**, B09401 (2006).

Acknowledgements

Part of this work was carried out at the Jet Propulsion Laboratory (JPL), California Institute of Technology, under a contract with the National Aeronautics and Space Administration (NASA), and financially supported through NASA's International Polar Year, GRACE Science Team and MEASUREs (through a project led by V. Zlotnicki in JPL) programmes. We thank Z. Altamimi, S. Bettadpur, J. Davis, I. Fukumori, F. Landerer, J. Ries, R. Riva, D. Salstein, M. Tamisiea and J. Wahr for discussions and help, and Y. Xu for editorial assistance. The figures are prepared using the GMT graphics package (Wessel and Smith, *EOS*, 1991).

Author contributions

X.W. formulated the project, conducted the inverse analysis and wrote the paper. M.B.H. produced the JPL GPS time series and participated in work formulation. H.S. and B.L.A.V. provided the viscoelastic deformation code and contributed to forward modelling of GIA. R.S.G. participated in work formulation and worked on consistency of gravity and polar-wander data. E.R.I. provided the IJ05 model and contributed to work formulation. D.D., A.W.M. and S.E.O. contributed to GPS data processing. All authors read the manuscript and discussed the results.

Additional information

The authors declare no competing financial interests. Supplementary information accompanies this paper on www.nature.com/naturegeoscience. Reprints and permissions information is available online at <http://npg.nature.com/reprintsandpermissions>. Correspondence and requests for materials should be addressed to X.W.